Available online at www.sciencedirect.com

SciVerse ScienceDirect

Ceramics International 39 (2013) 5031–5037

CERAMICS INTERNATIONAL

www.elsevier.com/locate/ceramint

Dual fiber behavior of polyvinyl alcohol/zirconium n-propoxide composite fibrous mats prepared via electrospinning

Sarabjit Singh*, Vajinder Singh, M. Vijayakumar, V.V. Bhanu Prasad

Defence Metallurgical Research Laboratory, P.O. Kanchanbagh, Hyderabad 500058, India

Received 9 October 2012; received in revised form 2 November 2012; accepted 29 November 2012
Available online 7 December 2012

Abstract

The electrospinning technique has been used to prepare composite fibrous mats of polyvinyl alcohol and zirconium n-propoxide. A halide-free synthesis route was adopted to prepare sol of zirconium n-propoxide. The fiber mats were deposited under different process parameters (applied voltage, needle–collector distance and flow rate). Two distinct regions have been noticed in the each fibrous mat for every specific process parameter. The microstructural change in the outer as well as in the inner regions of the composite fibers has been characterized by scanning electron microscopy. The process parameters significantly affect the fiber morphology of both the distinct regions. Outer region fibers showed least beaded morphology and more uniformity in the fiber diameter throughout their length. The average fiber diameter in the inner and outer regions was found to be in the range of 130–225 nm & 115–180 nm, respectively, under the different process parameters.

Keywords: B: Composites; B: Electron microscopy; B: Fibers

1. Introduction

The electrospinning technique is a low cost process for making fibers of variety of materials *viz*. polymers, metals, ceramics and their composites. The fibers made out of this process find their use in variety of applications like tissue engineering, sensor technology, capacitors and catalysis etc. because of their high surface area, high surface area to volume ratio and low weight [1–4]. This novel process is briefly described as follows: a polymer solution of required material is filled in the syringe fitted with a metallic needle of known diameter. This solution is driven from the syringe at a constant flow rate. High voltage is applied at the tip of the needle. When the voltage overcomes the surface tension of the solution drop, then the drop deforms into a conical shape. After exceeding a threshold value, the ejection of a liquid jet from the orifice takes place followed by a rapid bending and whipping processes in which the jet is continuously stretched and elongated by electrostatic repulsive forces. This leads to the formation of long, thin and uniform fibers and these fibers will ultimately collect on the surface of the conducting collector as result of electrostatic attractions.

Various ceramic oxide/polymer composite fibers have been prepared by mixing of polymer solution of adequate concentration to give sufficient viscosity to the ceramic oxide sol followed by electrospinning. The electrospinning process was performed by varying solution and process parameters and ambient conditions to get good quality bead-free fibers with nearly uniform diameter throughout their length. Different types of polymers like PVA (polyvinyl alcohol), PVP (polyvinyl pyrrolidone), PVAc (polyvinyl acetate) etc. have been used as a carrier material [5–9]. PVA, being hydrophilic, non-toxic and easy processing nature, finds its use in the electrospinning process to form fibrous films containing fibers with submicron to nanometer range [10–14]. Since good quality PVA/Zr n-propoxide composite fibers lead further to ZrO_2 fibers after the removal of PVA, it is very important to get the

*Corresponding author. Tel.: +91 40 245 86842; fax: +91 40 243 40683.
E-mail addresses: sarabdrdo@gmail.com, sarabjit@dmrl.drdo.in (S. Singh).

0272-8842/$ - see front matter © 2012 Elsevier Ltd and Techna Group S.r.l. All rights reserved.
http://dx.doi.org/10.1016/j.ceramint.2012.11.101

composite fibers with better morphology. These ZrO_2 fibers find applications in the areas of ceramic biomaterials, thermal barrier coatings, sensors etc. [15–17]. Hence, in the present work, composite fibers of PVA and Zr n-propoxide were prepared under different process parameters and carefully examined in detail to get their morphological features. For the sol preparation, Zr n-propoxide was used instead of zirconium oxychloride due to major two reasons: (i) to avoid chloride ions during processing which otherwise further lead to the formation of corrosive HCl gas during the heat-treatment and (ii) to get rid of the requirement of inert atmosphere [18,19]. As the nature of ZrO_2 fibers will depend exclusively on the as spun fibrous mat of PVA/Zr n-propoxide composite, hence, the morphology of fibers present in the composite fibrous mats prepared under various process conditions has been carefully examined.

2. Experimental details

The composite fibrous mats of PVA and Zr n-propoxide were prepared by using zirconium n-propoxide (analytical grade, Alfa-Aesar), poly (vinylalcohol) (PVA, MW = 1,25,000 and Degree of hydrolysis = 86–89%), acetyl acetone (Sigma Aldrich) and 2-methoxy ethanol (Sigma Aldrich) as the raw materials. An aqueous PVA solution of 6 wt% was prepared by dissolving a weighed amount of PVA powder in deionized water at 85 °C with constant stirring for ~2 h. Stable sol of Zr n-propoxide was prepared in anhydrated methoxy ethanol (refluxed at 120 °C) and acetyl acetone followed by the addition of dilute HNO_3 acid. Acetyl acetone served as a stabilizer and dilutes HNO_3 helped to increase the polarity of the medium. The electrospinning (ES) setup is manufactured by TSPL Pvt. Ltd., Secunderabad, India. This setup broadly consists of precisely programmable microprocessor based infusion syringe pump IP607, high voltage dc power supply and aluminum made collector plate. This collector plate was covered with aluminum foil and kept at 90° to the needle to collect the fibers during the process. The syringe (capacity of 2 ml) was filled with PVA/Zr n-propoxide composite solution (volume ratio of 4:1).

To study the effects of process parameters (electric potential, collection distance and solution flow rate) on the composite fiber morphology and diameters, fibers of PVA/Zr n-propoxide composite were synthesized under following different electrospinning conditions: voltage in the range of 11–15 kV, needle–collector distance in the range of 4.5–8.5 cm and flow rates in the range of 4.5–12.5 μL/min. All of these experiments were carried out for fixed collection time of 1 min keeping the collector in stationary mode. The digital images were captured for each fibrous mat prepared under all the three variable process parameters. As-prepared fibers of PVA/Zr n-propoxide composite were characterized by scanning electron microscopy (SEM). SEM images of the fibers were recorded by using FEI Quanta 400 scanning electron microscope. Fiber diameter was determined from the SEM images of fibers using the UTHSCSA Image tool software. For each experimental condition, the diameters of fifty different fibers were measured.

3. Results and discussions

Two distinct regions were observed in all the fiber mats deposited under different electrospinning process parameters. Fig. 1 shows the typical digital picture of PVA/Zr n-propoxide composite fibrous mat in which two distinct regions (referred as inner and outer) are differentiated by white color contrast. Sections 3.1 and 3.2 describe the effect of process parameters (applied voltage, needle–collector distance and flow rate) on the fiber morphology of the outer region and inner region, respectively. The analysis of average fiber diameter and the fiber size distribution of both the regions has been given in Section 3.3.

3.1. Analysis of outer region fibrous mat portion

Fiber morphology in the outer regions of as-spun composite fibrous mats deposited under variable applied voltage, needle–collector distance (NCD) and flow rates has been shown in Fig. 2(a–c), (d–f) and (g–i), respectively. The arrows shown in the figure indicate the ascending trend of each variable process parameter. The effect of increase of applied voltage on the fiber morphology is as follows: the composite fiber mats were deposited under following electrospinning conditions: the variable applied voltage of 11–15 kV (in steps of 2 kV) [Fig. 2(a–c)], the spinning solution flow rate of 8.5 μL/min and NCD of 4.5 cm. The fibers deposited at 11 kV show beaded as well as mesh-like behavior in their junctions. As we increase the voltage up to 13 kV, nearly bead free fiber morphology with complete drying behavior is observed. Fiber density is found to increase with increase in the applied voltage. Also, at 15 kV, again some stretchable beads along with interconnected junctions have appeared. The underlying mechanism for the changes observed in the fiber morphology has been proposed in the following: at the outset, with the increase in applied voltage, a conical shape droplet will form at the tip of the needle (Taylor cone). This cone

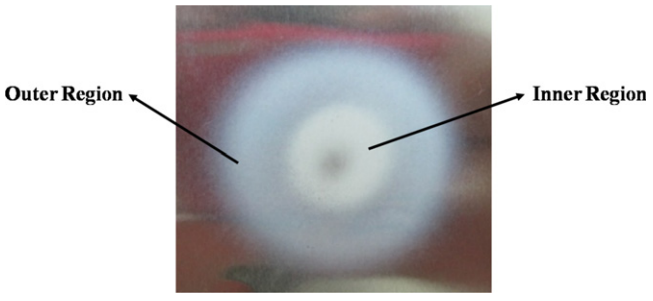

Fig. 1. Typical digital picture of PVA/Zr n-propoxide composite fibrous mat.

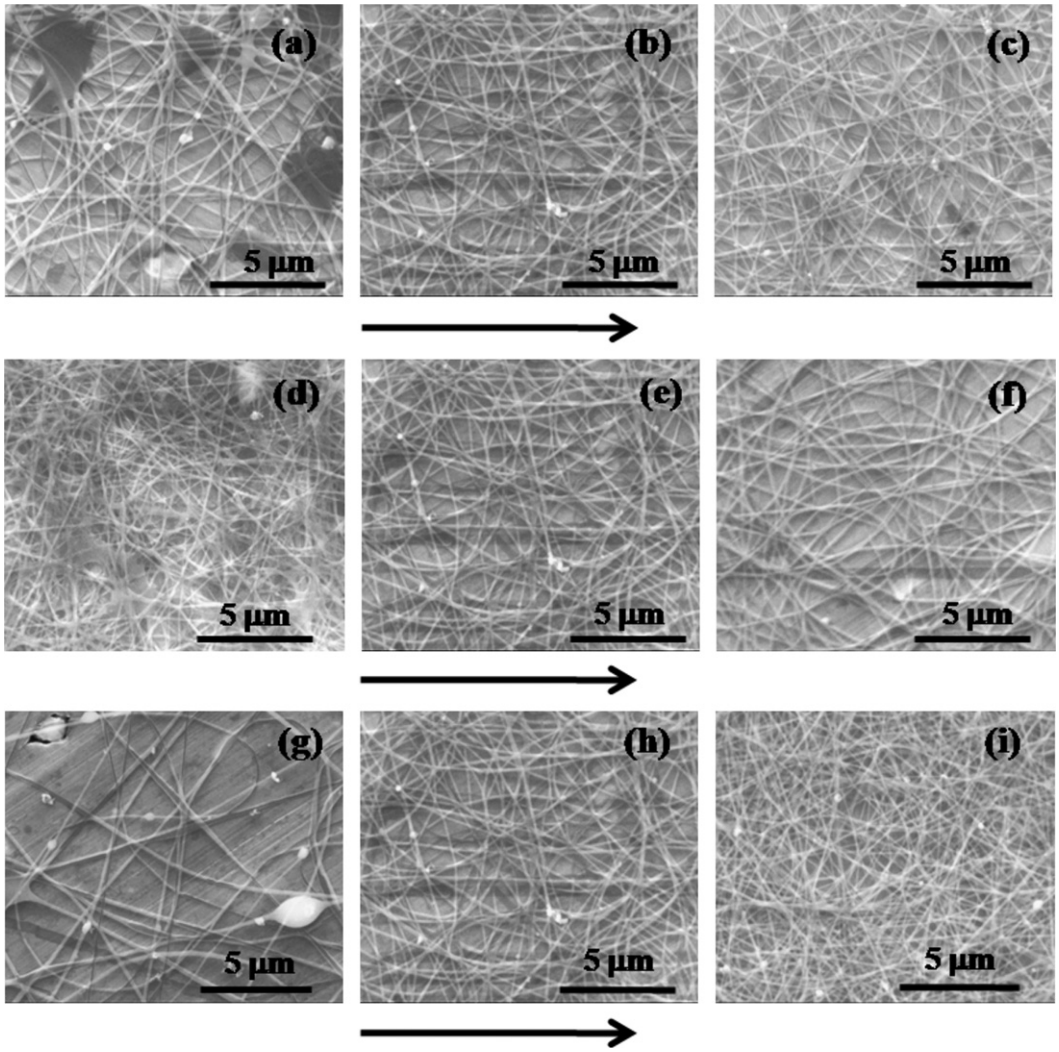

Fig. 2. The SEM micrographs for outer regions of the as-spun fibrous mats deposited under variable applied voltage: 11, 13 & 15 kV (a–c), NCD: 3.5, 4.5 & 7.5 cm (d–f), flow rate: 4.5, 8.5 & 12.5 μl/min (g–i). Arrow indicates the ascending order in all the three variables.

results into the initiation of the jet as a result of further increase in the electric field between the needle tip and the collector plate [20]. At lower applied voltage (11 kV), reduction in the Coulombic force occurs that dominates the effects of viscoelastic and surface tension forces (responsible for the beaded nature). With increase in the voltage (13 kV), Coulombic force further increases as a result of the more charge carriers. Therefore, jet segment experiences more stretching which results in the reduction of bead formation. But further increase in the voltage (15 kV) increases the jet instability as a result of receding of Taylor cone into the needle and again the beaded morphology will appear along with non-uniform fibers [21–23]. Thus, 13 kV is the optimum voltage to get uniform electrospun composite fibers with non-beaded morphology. Hence, conclusively, we can say that in order to get bead-free uniform fibers, the amount of applied voltage should neither be too low nor too high.

The effect of variable NCD on the fiber morphology is as follows: the electrospinning was performed by keeping fixed values of applied voltage (13 kV) and flow rate (8.5 μL/min), but at different needle-to-collector distance (in the range of 3.5 cm to 7.5 cm). It has been observed from the SEM micrographs [Fig. 2(d-f)] that the fiber density decreases with increase in NCD. The SEM micrograph of the fiber mat, which is deposited at least NCD of 3.5 cm, shows various diffused junctions at the connecting points. This is an indication of incomplete drying of the fiber jet prior to the deposition. With further increase of the NCD value to 4.5 cm, these junctions disappear and the fibers show isolating morphology. In the SEM micrograph for the highest NCD of 7.5 cm, although the fibers are mostly bead free, but the density is very less. Hence, the intermediate NCD i.e. 4.5 cm is found to be optimum because fibrous mat deposited at this distance under fixed value of applied voltage and flow rate shows dense fibers along with bead-free nature.

Effect of variable flow rate on the fiber morphology can be understood in the following way: to observe the effect of flow rate variation, the electrospun PVA/Zr

n-propoxide fiber mats were deposited under fixed applied voltage (13 kV), fixed NCD (4.5 cm) but at different flow rates (in the range of 4.5 μL/min to 12.5 μL/min). The fibers deposited at least flow rate (4.5 μl/min) show very poor morphology (Fig. 2g), whereas the fibers deposited at highest flow rate (12.5 μl/min) show beaded behavior (Fig. 2i). Beads are found to be spherical in-shape and they get stretched along with the fiber length with increase in the flow rate. Bead-free fiber morphology and diameter uniformity along their length (Fig. 2h) is observed for the fibrous mat deposited at intermediate flow rate (8.5 μl/min). Beaded fiber morphology at highest flow rate and improper fiber formation along with beaded nature at the least flow rate can be explained as follows: for a given value of applied voltage, there should be a corresponding moderate flow rate. Lower flow rate (4.5 μL/min) degrades the fibrous nature because the amount of solution, which is required to be spun, will be less. Also, if the flow rate is relatively high (12.5 μL/min), then the whole solution, which is coming out of the needle, will not completely converted into the fibers. Some part of it will drop on the ground due to gravitational effect without stretching. This in turn will disturb the morphology of already stretched fibers and finally results in the unstable jet. Therefore, flow rate should not be too low or too high, it should be moderate for a given value of applied voltage and NCD.

3.2. Analysis of inner region fibrous mat portion

The morphology of fibers deposited in the inner region of the fibrous mats at variable process parameters has been shown in Fig. 3. The effect of variable voltage (11–15 kV; in steps of 2 kV) on the fiber morphology is reflected by the SEM micrographs in Fig. 3(a–c). The value of flow rate and NCD was fixed at 8.5 μl/min and 4.5 cm, respectively. All the three fibrous structures show a beaded morphology with varying number of beads. Their morphology also varies with increase in voltage. The fibers deposited at

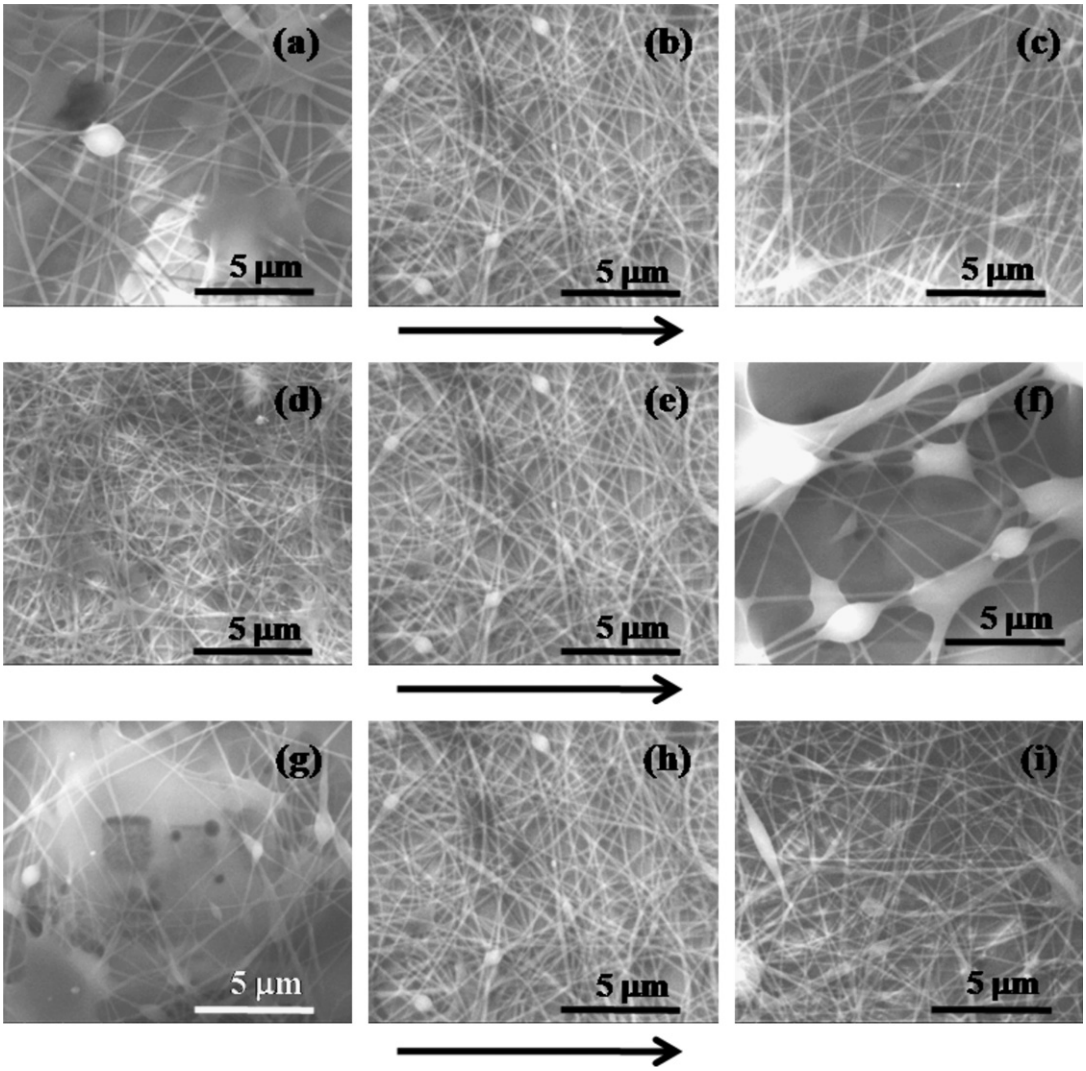

Fig. 3. The SEM micrographs for inner regions of the as-spun fibrous mats deposited under variable applied voltage: 11, 13 & 15 kV (a–c), NCD: 3.5, 4.5 & 7.5 cm (d–f), flow rate: 4.5, 8.5 & 12.5 μl/min (g–i). Arrow indicates the ascending order in all the three variables.

15 kV (maximum voltage) show elongated/stretched beads whereas the large size spherical beads and poor fiber morphology with jelly-like (non-dried) behavior along the fiber junctions can be seen for 11 kV (minimum voltage). Elongation of the beads at 15 kV occurs due to the increased starching force exerting on the jet segment. The fibers deposited at intermediate voltage of 13 kV show a relatively dense network with least number of beads, in comparison to the fibrous mat deposited at 15 kV. Also, the fibers possess nearly uniform diameter along their length suggesting that 13 kV is the optimum voltage for getting good quality fibers in the inner region of the fibrous mat.

The fiber morphology as a function of variable NCD (3.5–7.5 cm) is shown in Fig. 3(d–f). Voltage and flow rate conditions were kept as 13 kV and 8.5 μl/min, respectively. The fibers deposited at NCD of 3.5 cm and 4.5 cm show better morphology as compared to one at 7.5 cm. Completely dried fibers are observed for NCD of 4.5 cm whereas other two mats, deposited at 3.5 cm and 7.5 cm, show a non-dried fibrous behavior with jelly-like cloudy portions. These portions are more for the fibers deposited at NCD of 7.5 cm, which indicates poor morphology. The fibers deposited at small NCD (3.5 cm) do not get enough time to dry and at highest NCD (7.5 cm), electrospinning does not occur properly. However, it is quite surprising that good quality fibers are deposited in the outer region for highest NCD i.e. 7.5 cm, though in relatively small density. The SEM micrographs also suggest that fiber density decreases significantly with the increase in NCD from 3.5 cm to 7.5 cm, which is as expected in the electrospinning process.

The morphology of composite fibers as a function of variable flow rates is shown in Fig. 3(g–i). Voltage and NCD were kept at fixed values of 13 kV and 4.5 cm, respectively. The fibers deposited at low flow rate of 4.5 μl/min show incomplete formation with significant non-dried behavior. Not only relatively less non-dried nature is observed for the fibers deposited at highest flow rate of 12.5 μl/min but also elongated beaded morphology exits. The fibers deposited at intermediate flow rate of 8.5 μl/min show completely dried behavior along with only spherical beads. Also, the density of beads is smaller as compared to both the fibrous mats deposited at 4.5 μl/min and 12.5 μl/min. During the electrospinning process at 12.5 μl/min, it was noticed that the total amount of incoming solution from the needle was not fully converted into the fibers rather some part of it was getting wasted. This waste amount was disturbing the fibrous nature, which was originating from rest of the solution, hence, ultimately resulting in the elongated beads as well as some cloudy un-dried mesh.

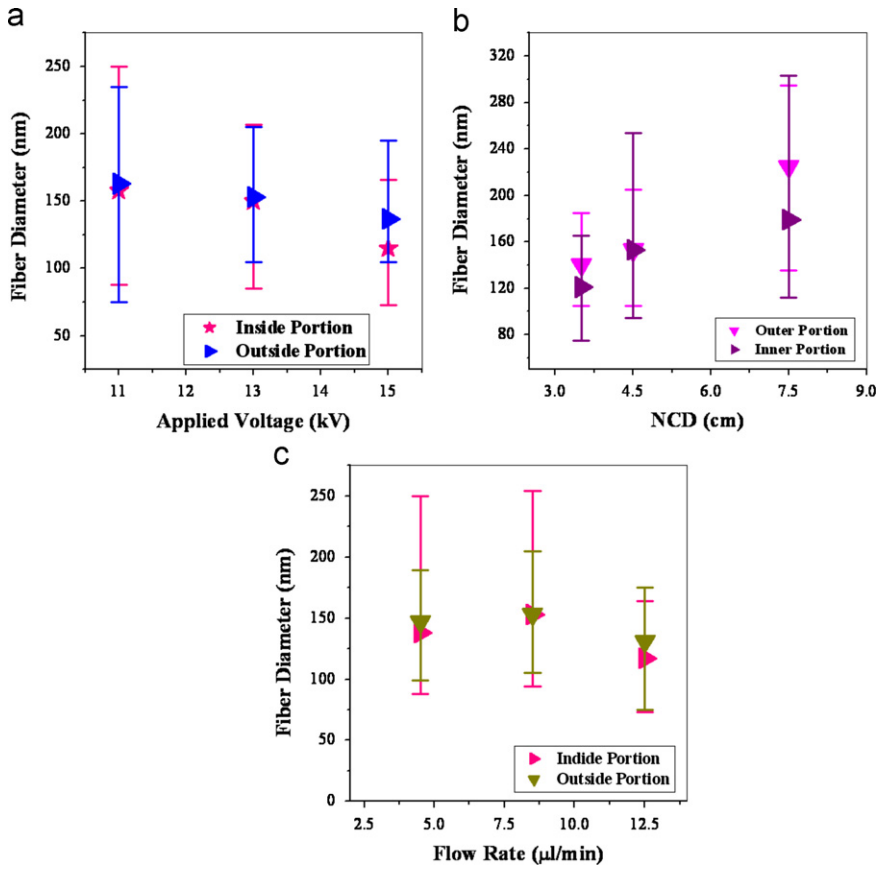

Fig. 4. Variation of fiber size distribution and average fiber diameter of the inner as well as the outer region fibers as a function of variable (a) applied voltage, (b) NCD and (c) flow rate.

3.3. Analysis of average fiber diameter (AFD) and the fiber size distribution (FSD) of outer and inner regions of the fibrous mats deposited at variable voltage, NCD and flow rate

Difference in the trend of fiber diameter as a function of applied voltage, NCD and flow rate for inner and outer region fibers have been summarized in Fig. 4a, b and c, respectively. The trend of AFD and FSD was found to be the same for the fibers deposited in both the regions. Both show decrease in their value with increase in the voltage from 11 kV to 15 kV. The trend in Fig. 4a illustrates that the variation in fiber diameter is less for outer region as compared to the inner region for every value of applied voltage. The fibrous mat deposited at 15 kV shows small AFD (137 nm) with FSD of 105–205 nm, whereas 11 kV sample shows relatively high AFD (163 nm) with FSD of 75–235 nm. If we analyze the inner portion, AFD varies from 158 nm for 11 kV to 115 nm and the FSD varies from 88 to 250 nm for 11 kV to 73–166 nm for 15 kV of applied voltage. The decreasing trend of AFD with increasing applied voltage results from the large columbic forces as well as strong electric field experienced by the solution drop, which comes out of the tip of the needle at a fixed flow rate. Hence, more stretching is faced by the fibers resulting into fine diameter. Similar effect of variable voltage has also been reflected in various studies of electrospinning [21,24–26].

The results of NCD variation (Fig. 4b) show that for both the regions, AFD as well as FSD increase with increase in the NCD from 3.5 cm to 7.5 cm. The AFD increase for the fibers present in the outer region is on the higher side as compared to those for the fibers present in the inner region. The FSD in case of inner region fibers shows the higher regime for each value of the NCD. Maximum size distribution for NCD of 7.5 cm of the outer region (135–295 nm) as compared to the inner region (112–303 nm) indicates the lower variation in the fiber diameter of the outer region fibers. The fibrous mat deposited at 7.5 cm shows high AFD (225 nm) having FSD of 135–295 nm, whereas the deposition at 3.5 cm resulted into relatively small AFD (133 nm) with FSD of 85–195 nm. For the inner region, fibers deposited at NCD of 3.5 cm show AFD of 121 nm with FSD of 75–165 nm, whereas the fibers deposited at 7.5 cm showed AFD of 180 nm with FSD of 112–303 nm. The increase in AFD as a function of increase of NCD can be explained as: when the NCD is increased, voltage applied per unit length i.e., electric field strength decreases and lesser electrostatic repulsive force is experienced by the composite polymer solution jet which is being discharged. Hence, jet velocity will decrease which further resulted in less stretching of the solution droplet, coming out of the needle, resulting in the increase in AFD of the PVA/Zr n-propoxide composite fibers [5,27].

Fig. 4c shows that the variation of AFD as well as FSD as a function of flow rate for outer region fibers is not so significant as compared to that for inner region fibers. The trend of AFD variation is found to be the same for both the outer as well as inner regions. The study of variable flow rates indicates that the fibers in the outer region have less diameter variation as compared to that of inner region. Outer region of the fibrous mat deposited at 12.5 μl/min shows least AFD value of 130 nm with size distribution of 75–175 nm. There is not much change in the AFD of fibers deposited at 4.5 μl/min and 8.5 μl/min flow rates. The AFD value of 147 nm with size distribution of 105–205 nm and 153 nm with size distribution of 105–195 nm was observed for 4.5 μl/min and 8.5 μl/min, respectively. The FSD shows decreasing trend as we increase the flow rate from 4.5 μl/min to 12.5 μl/min. For the inner region, significant variation in the AFD is observed for the fibers deposited at all the three flow rates. First, while moving from 4.5 μl/min to 8.5 μl/min, the AFD shows an increase in its value from 138 nm to 153 nm followed by significant decrease upto 117 nm for 12.5 μl/min. Fiber size distribution also showed a significant decrease for flow rate of 12.5 μl/min. Fibrous mat deposited at flow rate of 4.5 μl/min shows broad fiber size distribution (88–250 nm), whereas a significant narrow size distribution (73–164 nm) is observed for the fibrous mat deposited at flow rate of 12.5 μl/min.

In general, for every deposition condition, the AFD of outer region fibers is noticed to be more than the AFD of inner region fibers. This behavior may be described in terms of difference in the solidification rate. The fibers present in the outer region may dry rapidly because of the solvent evaporation at higher rate as compared to the fibers present in the inner region. This is due to the variable distance (from needle tip to the inner region and the outer region). This difference in the evaporation rate occurred due to large surface area produced as a result of more bending instability in the case of outer region fibers. Hence, the jet in this region solidifies fast and restricts the thinning behavior of the fibers, which ultimately results into an increase in the fiber diameter as well as AFD.

4. Conclusions

The composite fibrous mats of polyvinyl alcohol (PVA) and zirconium (Zr) n-propoxide were prepared by using the halide-free sol. The electrospinning process was performed under variable applied voltage, NCD and flow rates. Two distinct regions were observed for each process parameter. Both the regions were characterized for their fibrous morphological bahaviour including beaded/non-beaded nature, type of beads, fiber size distribution and average fiber diameter variation. Significant change was observed in the morphology of fibers deposited in the inner as well as outer regions. Relatively more beaded fibrous behavior was observed for the inner region fibers as compared to the outer region ones. Average fiber diameter of the outer region fibers showed higher values as compared to that of inner region fibers for all the process parameters, which may be resulted due to the difference in the solidification rate.

Acknowledgments

Authors gratefully acknowledge Dr. G. Malakondaiah, Director, Defence Metallurgical Research Laboratory (DMRL), Hyderabad for giving permission to publish the work. Authors are also thankful to Dr. Amol A. Gokhale, Outstanding Scientist, DMRL, Hyderabad for spending his precious time to examine the manuscript. Authors would also like to thank Dr. P. Ghosal, Scientist, DMRL, Hyderabad for providing the access of SEM facility besides the regular schedule and Dr. Subir Roy, Scientist, DMRL, Hyderabad for helping in the sol preparation.

References

[1] X. Song, Q. Qi, T. Zhang, C. Wang, A humidity sensor based on KCl-doped SnO_2 nanofibers, Sensors and Actuators B 138 (2009) 368–373.
[2] T.H. Cho, M. Tanaka, H. Onishi, Y. Kondo, T. Nakamura, H. Yamazaki, S. Tanase, T. Sakai, Battery performances and thermal stability of polyacrylonitrile nano-fiber-based nonwoven separators for Li-ion battery, Journal of Power Sources 181 (2008) 155–160.
[3] X. Song, L. Liu, Characterization of electrospun ZnO–SnO_2 nanofibers for ethanol sensor, Sensors and Actuators A 154 (2009) 175–179.
[4] D.R. Nisbet, J.S. Forsythe, W. Shen, D.I. Finkelstein, M.K. Horne, Review Paper: a review of the cellular response on electrospun nanofibers for tissue engineering, Journal of Biomaterials Applications 24 (2009) 7–29.
[5] F.R. Lamastra, A. Bianco, A. Meriggi, G. Montesperelli, F. Nanni, G. Gusmano, Nanohybrid PVA/ZrO_2 and PVA/Al_2O_3 electrospun mats, Chemical Engineering Journal 145 (2008) 169–175.
[6] H. Guan, C. Shao, S. Wen, B. Chen, J. Gong, X. Yang, A novel method for preparing Co_3O_4 nanofibers by using electrospun PVA/cobalt acetate composite fibers as precursor, Materials Chemistry and Physics 82 (2003) 1002–1006.
[7] H. Guan, W. Zhou, S. Fu, C. Shao, Y. Liu, Electrospun nanofibers of NiO/SiO_2 composite, Journal of Physics and Chemistry of Solids 70 (2009) 1374–1377.
[8] X. Zhang, S. Xu, G. Han, Fabrication and photocatalytic activity of TiO_2 nanofiber membrane, Materials Letters 63 (2009) 1761–1763.
[9] H. Guan, C. Shao, Y. Liu, N. Yu, X. Yang, Fabrication of $NiCo_2O_4$ nanofibers by electrospinning, Solid State Communications 131 (2004) 107–109.
[10] M. Krumova, D. López, R. Benavente, C. Mijangos, J.M. Pereña, Effect of crosslinking on the mechanical and thermal properties of poly(vinyl alcohol), Polymer 41 (2000) 9265–9272.
[11] V. Gimenez, A. Mantecon, V. Cadiz, Modification of Poly-(vinyl alcohol) with acid-chlorides and crosslinking with difunctional hardeners, Journal of Polymer Science: Polymer Chemistry Edition 34 (1996) 925–934.
[12] P. Supaphol, S. Chuangchote, On the electrospinning of poly(vinyl alcohol) nanofiber mats: a revisit, Journal of Applied Polymer Science 108 (2008) 969–978.
[13] W.K. Son, J.H. Youk, T.S. Lee, W.H. Park, Effect of pH on electrospinning of poly(vinyl alcohol), Materials Letters 59 (2005) 1571–1575.
[14] E. Yang, X. Qin, S. Wang, Electrospun crosslinked polyvinyl alcohol membrane, Materials Letters 62 (2008) 3555–3557.
[15] P. Charpentier, P. Fragnaud, D.M. Schleich, E. Gehain, Preparation of thin film SOFCs working at reduced temperature, Solid State Ionics 135 (2000) 373–377.
[16] D.R. Clarke, C.G. Levi, Materials design for the next generation thermal barrier coatings, Annual Review of Materials Research 33 (2003) 383–417.
[17] C. Piconi, G. Maccauro, Zirconia as a ceramic biomaterial, Biomaterials 20 (1991) 1–25.
[18] G. Pfaff, A novel reaction path to barium zirconates by the decomposition of peroxide precursors, Materials Letters 24 (1995) 393–397.
[19] G. Pfaff, Synthesis of magnesium stannates by thermal decomposition of peroxo precursors, Thermochimica Acta 237 (1994) 83–100.
[20] D.H. Reneker, I. Chun, Nanometer diameter fibers of polymer produced by electrospinning, Nanotechnology 7 (1996) 216–223.
[21] J.M. Deitzel, J. Kleinmeyer, D. Harris, N.C.B. Tan, The effect of processing variables on the morphology of electrospun nanofibers and textiles, Polymer 42 (2001) 261–272.
[22] X.H. Zhong, K.S. Kim, D.F. Fang, S.F. Ran, B.S. Hsiao, B. Chu, Structure and process relationship of electrospun bioabsorbable nanofibers membranes, Polymer 43 (2002) 4403–4412.
[23] T. Jarusuwannapoom, W. Hongrojjanawiwat, S. Jitjaicham, L. Wannatong, M. Nithitanakul, C. Pattamaprom, P. Koombhongse, R. Rangkupan, P. Supaphol, Effect of solvents on electro-spinnability of polystyrene solutions and morphological appearance of resulting electrospun polystyrene fibers, European Polymer Journal 41 (2005) 409–421.
[24] J.S. Lee, K.H. Choi, H.D. Ghim, S.S. Kim, D.H. Chun, H.Y. Kim, W.S. Lyoo, Role of molecular weight of atactic Poly(vinyl alcohol) (PVA) in the structure and properties of PVA nanofabric prepared by electrospinning, Journal of Applied Polymer Science 93 (2004) 1638–1646.
[25] S. Megelski, J.S. Stephens, D.B. Chase, J.F. Rabolt, Micro- and nanostructured surface morphology on electrospun polymer fibers, Macromolecules 35 (2002) 8456–8466.
[26] K.J. Pawlowski, H.L. Belvin, D.L. Raney, J. Su, J.S. Harrison, E.J. Siochi, Electrospinning of a micro-air vehicle wing skin, Polymer 44 (2003) 1309–1314.
[27] Y.C. Ahn, S.K. Park, G.T. Kim, Y.J. Hwang, C.G. Lee, H.S. Shin, J.K. Lee, Development of high efficiency nanofilters made of nanofibers, Current Applied Physics 6 (2006) 1030–1035.